*

New developments in low clinker cement paste mineralogy

M. Frías[1,*], R. Vigil de la Villa[2], R. García[2], S. Martínez-Ramírez[3], L. Fernández-Carrasco[4]

[1]Eduardo Torroja Institute for Construction Science (IETcc-CSIC), 28033 Madrid, Spain.

[2]Department of Geology and Geochemistry, CSIC-UAM Associated Unit (Geomateriales), Autonomous University of Madrid, 28049 Madrid, Spain.

[3]Institute for the Structure of Matter (IEM-CSIC), 28006 Madrid, Spain

[4]Department of Civil and Environmental Engineering, Barcelona TECH, 08034 Barcelona, Spain.

*Corresponding author: e-mail: mfrias@ietcc.csic.es, Tel +34913020440, Fax +34913020700

Abstract

The use of industrial waste as a cement addition often changes the composition and development of the hydrated phases and with them matrix performance and durability, in particular at later ages. The effect of the presence in blended cement of 20% to 50% Kaolinite based activated carbon waste (ACW) on paste hydration has been characterized by means of XRD, SEM/EDX, TG/DTG, NMR and FTIR to identify and monitor the mineralogical phases forming in materials at ages of up to 180 d. The results showed that the main reaction products forming in the first 7 d included C-S-H gels, C_4ACH_{12} and C_4AH_{13} (hydroxy-AFm). Whilst monocarboaluminate (Mc) content declined with rising percentages of ACW, the amount of hexagonal phase hydroxy-AFm rose generally speaking. Then microstructure of the C-S-H gels developing in the OPC and the 50% additioned paste differed. Compact C-S-H gel plates, and

phyllosilicate-like laminar spongy microplates with high polymerised C-S-H gel formed in the blended cement paste.

Keywords: mineralogy, hydrated phases, activated clay waste, blended cement

I. Introduction

The cement industry's standard reuse of large amounts of industrial waste and by-products as supplementary cementitious materials has a very beneficial effect on its sustainability as well as on socio-economic development. Not only does the end product have a smaller environmental footprint (lower CO_2 emissions) and lower energy consumption which translates into lower costs, but also improves upon cement performance (Juenger and Siddique, 2015; Stark, 2011; Medina et al. 2017; Mohammed et al., 2016; Wang et al., 2016). In keeping with European legislation on commercial cement manufacture (European Committee for Standardization, 2011) thermally activated pozzolans, whether natural or industrial (such as fly ash, silica fume or blast furnace slag), have traditionally been added to cement at replacement ratios (alone or mixed) of up to 55%, depending on the type of cement. Given that worldwide cement production stands at around 4.2 billion tonnes/year, with demand predicted to rise substantially by 2050, natural pozzolan consumption is expected to be very high. The scientific community is consequently exploring industrial by-products as a possible source of other types of pozzolanic materials.

Kaolinite-based waste has been the object of a recent line of research as an alternative to the kaolinite extracted from natural quarries (Chakchouk and Samet, 2012; Rodriguez et al., 2013; Frías et al., 2013; Frías, 2006). The sludge generated by the paper industry, which recycles paper into cellulose, is one such waste (Segui et al., 2012; Monte et al., 2009; Yan et al., 2011). Of the

55 over 14.4 million tonnes produced in Europe yearly, 70% is generated during
56 the manufacture of de-inked recycled paper. Earlier studies (Frías et al. 2015;
57 Vigil et al., 2007; Vegas et al., 2014; Goñi et al.,2013) laid the scientific-
58 technical grounds for converting kaolinite/calcite-based industrial waste to a
59 high pozzolanicity product, identifying the main hydrated phases to be C-S-H
60 gels, metastable hexagonal phases (hydroxy-AFm and C_2ASH_8), C_4ACH_{11} and
61 layered double hydroxide (LDH)-like structures such as carbonate and
62 metakaolinite (MK).
63 Research presently focuses on by-products such as coal mining waste
64 (kaolinite/mica) (Fan et al., 2014; Modarres and Ayar, 2014; Frías et al., 2012),
65 the stockpiling of which in areas around mines poses substantial environmental
66 problems (Haibin and Zhenling, 2010; Dontala et al., 2015). According to the
67 information available (BP Statistical Review of Wold Energy, 2017), worldwide
68 coal output amounted to 19.350 Gt in 2016, and the respective waste to 40% of
69 site production, depending on geology and mine conditions. When thermally
70 activated at 500°C to 900°C for 2 h, such clayey waste can be converted to a
71 metakaolinite-containing pozzolan, activated coal waste (ACW) (García et al.,
72 2015; Vigíl et al., 2017) although the activation conditions must be controlled to
73 prevent the formation of quasi-stable dehydroxylated mica (Vigil et al., 2014).
74 To date, research has focused on the pozzolanicity of ACW/lime system, in
75 which the hydrated phases identified include C-S-H gels, Hydroxy-AFm,
76 C_2ASH_8 and LDH-like phyllosilicate/carbonate structures. The use of coal waste
77 as a component in blended cements is a line of research scantly pursued by the
78 scientific community, with the few papers available all dealing with its technical
79 properties (Modarres et al., 2016; Beltramini et al., 2010; Vegas et al., 2015). In

a previous paper, Frias et al.,2016 reported the reaction kinetics of blended cement pastes containing up to 20% ACW. They identified C-S-H gels, ettringite (Et), hydroxy-AFm and C_4ACH_{12} as the phases primarily involved in the synergies between cement hydration and the pozzolanic reaction.

Insight into the behaviour of such binary cements, presently unknown, would contribute to a deeper understanding of low cement content and hence low CO_2 systems.

This study, the first to explore 20% to 50% activated coal waste cement hydration used XRD, SEM-EDX, TG/DTG, FTIR and NMR techniques to identify and monitor the hydrated phases in 1 d, 7 d, 28 d, 90 d and 180 d pastes.

II. Experimental

(1) Materials

Spanish coal mining waste from an open-pit mine (Sociedad Anónima Hullera Vasco-Leonesa, León) was thermally activated at what are generally regarded as optimal conditions (García et al., 2016): 600°C for 2 h in an electric muffle furnace. The product (ACW) was subsequently ground to particle sizes of under 90 µm.

Further to the requirements laid down by the European Committee for Standardization (2011) for the manufacture of type II A/B commercial cements, a CEM I 52.5R commercial portland cement was used in this study. The D_{90} (diameter through which 90 % of the product passes) for the cement was 35.9 µm and 32.6 µm for the waste. The chemical composition of the starting materials is given in Table I;

while the mineralogy by Rietveld of the starting materials is collected inTable II and the datasets for phase identification in Table III, using X^2 as an index of disagreement or goodness of fit to the quotient between Rwp and Rexp.

Table I. Chemical compositions (%) of OPC and ACW

Table II. Rietveld analysis of XRD-identified phases

Table III: Datasets for phase identification and Rietveld quantification

The blended cements contained 0%, 20%, 30% or 50% ACW. Prismatic (1x1x6 cm) cement paste specimens were prepared at a water/binder ratio of 0.5, to which 40% solid Sikament FF superplasticiser was added to attain the same fluidity as in the reference paste. The mixing water was corrected for the admixture water to maintain a constant water/binder ratio. All the specimens were cured in water for up to 180 days. After each curing period they were immersed in acetone for 24 h and vacuum dried for a further 24 h to stop cement hydration.

(2) Methods

The chemical composition of the starting ACW and OPC samples was analysed on a Philips (Eindhoven, Netherlands) PW 1404 X-ray fluorescence analyser fitted with an Sc-Mo X-ray tube and Super-Q Manager analytical software.

The mineralogical composition of the bulk samples was determined by random powder X-ray diffraction (XRD) on a Siemens D-5000 (Munich, Germany) X-ray diffractometer fitted with a Cu anode. Their operating conditions were 30 mA and40 kV and divergence of 2 and 0.6 mm with reception slits, respectively. The samples were scanned in (2θ) 0.041 steps with a 3-scount time.The characterization of bulk samples was carried out using the random power

131 method operating from 3º to 70º 2θ at a rate of 2º/min (Moore and Reynolds,
132 1997). The XRD patterns were analyzed with the Match 3 Rietvel Fullprof
133 software (Match, Fullprof) using the Inorganic Crystal Structure Database
134 (ICSD) (Allmann and Hinek, 2007) and the Crystallography Open Database
135 (COD) (Grazulis et al., 2012). Rietveld quantification (Rietveld, 1967,1969)
136 accuracy is typically presented in terms of constants R and X^2. While, R only
137 compares peak intensities calculated from the spectra of the material to the
138 intensity of the experimentally line, the X^2 calculation in phase weight as well.
139 Ideally, both constants should be equal to 1. Due to discrepancy between
140 observed and calculated data, however, which are particularly significant for
141 materials comprising more than three phases, X^2 values of 20 to 5 are generally
142 accepted as satisfactory for valid results.
143 In light of the optics of all the data gathering instruments used (including Bragg
144 Brentano geometry, Cu Kα1 wavelength, fixed divergence and Soller slits), the
145 pseudo-Voigt function was chosen as the most suitable to describe peak shape
146 in the preliminary fit performed. The information on the structural parameters
147 listed for the phases on their COD or ICSD cards was entered. The parameters
148 were refined in the recommended order (McCusker et al., 1999): first the global
149 parameters, i.e., background functions (the Chebyshev polynomial function,
150 using three variable coefficients), zero shift and scale factors, followed by the
151 unit cell parameters for each phase. The March-Dollase function, normally apt
152 for correcting preferred orientation in flat-plate specimens, was applied (Dollase,
153 1986). The instrumental polarisation factor (0.7998) and optics used in these
154 diffraction trials were applied to modify peak shape and isotropic and
155 anisotropic factors. Two corrections to optimise the fit were introduced during

the refinement cycles: for micro-absorption (Brindley, 1951) to minimise the effect of different absorption coefficients for the phases present in the mix and for diffraction peak alternations using the Caglioti equation (Caglioti, 1958).

Sample morphology and microanalysis were determined with SEM/EDX on an Inspect FEI electron microscope (Hillsboro, OR, USA), fitted with a W source, DX4i energy dispersive X-ray analyser and a Si (Li) detector. Freshly cut samples were observed using a backscattered electron (BSE) detector, whereas the gold-sputtered field samples were examined with a high-vacuum imaging secondary electron detector (resolution: 3.0 nm at 30 kV [ETD],10 nm at 3 kV [ETD], and 4.0 nm at 30 kV [BSE]). The accelerating voltage was 26-30 kV and the working distance 10 mm. Sample microanalysis was conducted on an Oxford Instruments INCA Energy 200 energy dispersive X-ray spectrometer, running at 20 kV. SEM-EDS precalibration tests were conducted with internal standards to improve ZAF correction. The chemical composition, found as the mean of 10 scans per sample, is shown in Table IV together with the standard deviation. These semi-quantitative analyses were performed on clean surfaces to prevent contamination as far as possible. The findings are expressed in wt% of oxides.

Sample particle size distribution was determined with a Malvern Mastersizer 3000 laser granulometer(Great Malvern, UK), with air as the dispersing medium (Frías and Sánchez de Rojas, 1997).

Thermogravimetric studies (TG/DTG) were conducted with an SDT Q600 V20.9 Build 20 analyser on 45 mg to 50 mg powder samples, heated at a rate of 10 °C/min in an N_2 (100 mL/min) atmosphere.

Pellets in which 1.2 mg of hydrated paste sample were mixed with 10 mg of potassium bromide were analysed on a Bruker Alpha infrared spectrometer. The spectra were recorded in the 4000 cm^{-1} to 400 cm^{-1} region at a resolution of 4 cm^{-1}.

The 180 d pastes were analysed on a Bruker Avance III 400 MHz nuclear magnetic resonance (NMR) mass spectrometer fitted with a 9.4 T magnet. ^{29}Si spectra were recorded at the following settings: resonance frequency, 79.49 MHz; spin rate, 10 kHz; single 5 µs pulse; recycle delay, 10 s; external standard, tetramethylsilane (TMS). ^{27}Al spectra were recorded at the following settings: resonance frequency, 104.3 MHz; spin rate, 10 kHz; single 2 µs pulse; recycle delay, 5 s; external standard, $Al(H_2O)_6^{3+}$.

III. Results and Discussion

Figure 1 shows the 180 d diffractograms with the mineralogical phases identified.

Rietveld quantification of the crystalline mineralogical phases in the four cements are given by age in Table II.

Table II. Rietveld analysis of XRD-identified phases

The anhydrous OPC consisted primarily in tricalcium silicate (alite), dicalcium silicate (bredigite), tricalcium aluminate, bassanite and a ferritic phase. The 1 d materials contained the most prominent crystalline phases, portlandite and ettringite, and exhibited a significant decline in anhydrous phases C_3S and C_3A compared to the anhidrous cement. The hydrated phase content, greater in the 7 d pastes, included tetracalcium aluminate monocarbonate hydrate (C_4ACH_{12}),

a line with an intensity that continued to rise up to 90 d of hydration. After 28 d of hydration the metastable hexagonal phase, tetracalcium aluminate hydrate (hydroxyl-AFm), was formed (4-7%). C_4ACH_{12}, product of a solid state mechanism-governed reaction between C_3A and $CaCO_3$, stabilised ettringite formation (Bonavetti et al., 2001; Feldman et al., 1965; Zajac et al., 2014).

The 1 d diffractograms for the mixed pastes contained the same lines as the anhydrous cement, along with reflections indicating the presence of the quartz and mica present in the ACW. This waste originally contained calcite and an amorphous phase in addition to quartz and a phengite-like mica.

As no product derived from the reaction between pozzolan and cement was observed at that age, it was assumed that the addition would act as a filler, accelerating the hydration of cement particles. That in turn induced a substantial (around 75%) decline in the alite and bredigite contents and a 20% rise in the portlandite content relative to the reference cement.

At later hydration ages the presence of ACW favoured C_4AH_{13} formation but not the monocarboaluminate generation observed in OPC. The appearance of an aluminium-high phase was attributed to the uptake of the reactive alumina present in the pozzolan (metakaolinite) (Frías et al., 2016; Wu and Young, 1984; Atkins et al., 1991).

Up to 28 d, the materials containing the pozzolan, particularly the 30 % and 50 % blended cements, had a higher proportion of amorphous phase than the control (Table III). Its presence began to decline after 90 d, in inverse proportion to the cement replacement ratio. That turning point in the amount of amorphous

material might be related to the excess pozzolan relative to the amount of portlandite generated by the portland cement.

The SEM/EDX scans of the OPC exhibited laminar hydrated portlandite and prismatic ettringite phases, in addition to short C-S-H gel fibres. Intertwined with the ettringite prisms, the gels occupied the voids surrounded by layers of portlandite and alite, which grew thicker with curing time. Adding 20% ACW to the OPC paste induced the formation of more compact laminar portlandite structures, along with ettringite and C-S-H gel fibres (Frías et al., 2016). The 180 d morphologies of the four cements analysed are shown in Figures 2-4. The pastes containing 0% and 20% ACW had dense, compact morphologies (Figure 2). The 30% and 50% blended pastes, in contrast, were characterised by spongy, scantly compact morphologies, differences that widened with rising ACW content and curing time (Fig. 3).

A detailed study of cement morphologies revealed two types of plates. a) Compact plates comprised C-S-H gel, in which a higher ACW content favoured a decline in calcium and a rise in silicon and aluminium contents. b) Less compact plates consisted in a mix of laminar and fibrous structures (Figure 4, left; Table IV). The laminar phyllosilicate microplates characterising the 50%ACW paste (Figure 4, right; Table IV) induced the aforementioned spongy, scantly compact morphology. The EDX analysis for the major mineralogical phases is shown in Figure 5.

Table IV. EDX chemical analysis of 180 d blended cements (%)

The SEM micrographs clearly attested to differences in paste morphology with the percentage of ACW added. At replacement ratios of over 20%, the matrices were neither uniform nor porous, a finding compatible with the evolution of the amorphous stage in these pozzolan-high cement pastes.

The high frequency region (4000 cm^{-1} to 3000 cm^{-1}) on the FTIR spectrum (Fig.6) contained a signal at 3645 cm^{-1} attributed to the OH stretching vibrations in portlandite. That band was more intense in the OPC sample and declined in intensity as the ACW content rose. OH stretching vibrations generated by water molecules were also detected, with peaks at around 3430 cm^{-1} and 3626 cm^{-1}, due to C-S-H gel. This wide band exhibited shoulders at 3673 cm^{-1}, 3667 cm^{-1}, 3642 cm^{-1}, 3625 cm^{-1} and 3522 cm^{-1} due to OH vibrations that grew in intensity with ACW content and curing age, most prominently in the 50% replacement samples. Inasmuch as C_4AH_{13}, ettringite and monocarboaluminate all have a band at those frequencies, these shoulders could be attributed to any or several of them. A signal appearing at 3529 cm^{-1} might denote the presence of aluminium hydroxides resulting from the formation or carbonation of calcium aluminates. As these hydroxides are amorphous, they would not be detected by XRD (Qoku et al; 2017).

In the FTIR study of the C-S-H gel formed, at lower frequencies, the OPC paste spectrum exhibited bands at around 1118 cm^{-1} and 973 cm^{-1}. Earlier authors (Yu et al.,1999) reported that the band at 973 cm^{-1} can be attributed to the stretching vibrations generated by the Si-O bonds in Q^2 tetrahedra present in C-S-H gel. This band clearly shifted toward higher wavenumbers in the presence

of ACW: 995 cm^{-1} with 20%, 1002 cm^{-1} with 30% and 1015 cm^{-1} with 50% additions (Fig. 7). A band that appeared at 1085 cm^{-1} possibly denoted a more polymerised structure. According to Sáez del Bosque et al. (2014), structures with a high Ca/Si ratio generate bands at 902 cm^{-1}, 964 cm^{-1}, 984 cm^{-1} and 1081 cm^{-1}, associated with the Q^2 stretching vibrations in Dreierkette-arranged silicates, whereas in structures with a low Ca/Si ratio the same units generate bands at around 1120 cm^{-1} and 969 cm^{-1}. In the spectra shown here, however, the signals at 798 cm^{-1}, 780 cm^{-1}, 696 cm^{-1}, 558 cm^{-1} and 480 cm^{-1} were attributed to ACW, which also generated Si-O bands at 1040 cm^{-1} and 1082 cm^{-1}.

^{27}Al and ^{29}Si NMR scans were recorded of the 180 d materials to determine whether those shifts were due to the existence of a different gel or to the effect of unreacted phases in the ACW.

The 180 d ^{29}Si NMR (Fig. 8) for all the pastes contained signals for Q^0 units at -71.5 ppm and -73.6 ppm, the intensity of which declined with rising percentages of pozzolan, for at lower percentages of cement its anhydrous phases C_2S and C_3S logically generated less intense signals. The most intense signal, positioned at -71.5 ppm, was attributed to β-C_2S, as C_2S hydration is slower than that of C_3S the intensity of the peak associated with the presence of C_2S is higher than that of C_3S. Other researchers (Kunter et al.,2016) calculating the percentage of alite and bredigite in white cement samples with a 5% to 30% metakaolin content, observed that as the percentage of MK rose, the amount of bredigite reacting declined substantially, whereas the effect on

306 alite was less accentuated. That would explain the intense bredigite signals on
307 the ^{29}Si NMR spectrum.
308
309 The decline in intensity with rising replacement ratios in the signals for the Q^1
310 units present in the hydrated phases denoted greater polymerisation of the C-S-
311 H gels, corroborating the FTIR and SEM findings. In the presence of the waste,
312 a Q^3 unit signal generated by the clayey minerals, primarily micas, present in
313 the ACW, appeared between -89 ppm and -97 ppm, growing in intensity with
314 the pozzolan content in the cement paste.
315 Q^2_B and Q^2_P signals were observed in the pastes in proportions that varied with
316 the replacement ratio, with the former declining as the ratio rose. The Q^2 (1Al)
317 units likewise detected denoted the presence of greater amounts of aluminium
318 from the ACW and the replacement of bridging silicon with aluminium atoms.
319 The 180 d ^{27}Al NMR spectra for the cement pastes containing 0%, 20%, 30%
320 and 50% ACW reproduced in Figure 9 contain two areas of signals attributable
321 to Al(IV) and Al(VI). The latter confirmed ettringite and monocarboaluminate
322 formation in all the samples, albeit in different proportions, as observed with
323 XRD. Raising cement replacement ratios raised the percentage of Mc and
324 lowered the amount of Et.
325 The intensity of the wide signal observed in the area of the spectrum attributed
326 to tetrahedral aluminium rose with the amount of waste added. That signal,
327 peaking at 68.6 ppm and shifting to lower values with higher replacement ratios,
328 was indicative of the presence of Al uptake in the C-S-H gel. Moreover, the
329 shoulder with a well-defined peak appearing at 61.5 ppm in this area of the

spectrum for the paste containing 50% ACW might be related to the SEM-identified laminar phyllosilicate microplates in that material.

The OPC and 50% ACW DTG curves up to 180d are shown in Figure 10, by way of example of all the blended cements analysed (0%, 20%, 30% and 50% ACW), exhibit three distinct areas with significant weight loss.

1. The wide band at 70°C to 300°C was generated by dehydroxylation of the main hydrated phases during both cement hydration and the pozzolanic reaction. Bearing these two reactions in mind, the most prominent band (outside of the one at 61°C to 65°C attributed to the loss of moisture in the samples), located at 70°C to 135°C and peaking at 102°C to 106°C, would be associated with ettringite and especially C-S-H gel dehydroxylation. A less intense band in the 130°C to 210°C interval was attributed to several hydrated phases with overlapping signals: hydroxy-AFm (180°C), C_4ASH_{12} (170ºC) in the 90 d and 180 d blended cements with 50% ACW and carboaluminate hydrate (C_4ACH_{12}) (190°C to 210ºC) (Martínez and Frías, 2011). Those findings corroborated the presence of the hydrated phases observed with XRD, FTIR, SEM and NMR.
2. As the thermogravimetric interval ranging from 400°C to 470°C, peaking at 430°C to 445°C, was generated by the dehydroxylation of portlandite present in the cements, band intensity was greater at lower ACW percentages (OPC >20%ACW >30%ACW >50%ACW), as observed in the FTIR analyses.
3. The area between 550°C and 740°C, with a peak at around 700°C to 705°C, was associated with calcite decarbonation in the blended cements.

Weight loss due to hydrated phase dehydroxylation at 70°C to 300°C is graphed against portlandite content (in percent of $Ca(OH)_2$) and cement age in Figure 11. The graph clearly shows that the $Ca(OH)_2$ content declined as the percentage of coal waste rose due to the pozzolanic reaction between the MK present in the ACW and the portlandite generated in cement hydration. The portlandite content in OPC was 13% to 16%; in 20%ACW, 11% to 12.5%; in 30%ACW, 9 to 9.5%; and in 50%ACW from 5% to 6.5%.

The greatest bound water loss (hydrated phase dehydroxylation in the 70°C to 300°C range) was observed at 28 d in OPC and 20%ACW and at 90 d in 30%ACW and 50%ACW. A slight decline in bound water content was detected at longer reaction times, perhaps associated with the presence of majority hydrated phases such as hydroxy-AFm, with a lower water molecule content in their structure than found in early age-forming ettringite ($C_6AS_3H_{32}$).

IV. Conclusions

The instrumental techniques applied in this study to appraise the hydration of binary cements with a low clinker content showed that the partial replacement of cement with 20 wt% to 50 wt% ACW favoured the formation of hydroxy-AFm, a metastable crystalline phase, over monocarboaluminate (C_4ACH_{12}) (4% to 12 %). The former may account for up to 20% of all the crystalline phases, peaking in 28 d 20%ACW cement paste and subsequently declining with rising pozzolan content. In the OPC paste, monocarboaluminate prevailed over hydroxy-AFm (4% to 7%), peaking at 17% of the total in the 90 d and declining slightly in the 180 d paste.

Two types of plates were distinguished with the addition of pozzolan: compact C-S-H gel plates, and phyllosilicate-like laminar spongy microplates, the presence of which grew with pozzolan content, most visibly in the 50%ACW paste.

Silicon is partially replaced by aluminium during C-S-H gel polymerisation, as attested to by the band shift to higher frequencies (950→1015 cm^{-1}) and FTIR (Si-O Q^2 stretching vibrations) and NMR (Q^2 (1Al)) findings. Further research would be required to confirm whether those developments have a beneficial effect on the performance of ACW blended cements, and its possible benefits with respect to other cement matrices.

Acknowledgements

This research was funded by the Spanish Ministry of Economy and Competitiveness (BIA2015-65558-C3-1-2-3R) (MINECO/FEDER)). The assistance received from Sociedad Anónima Hullera Vasco-Leonesa, SIKA (Madrid, Spain) and the Spanish Cement Institute (IECA) for this study is gratefully acknowledged.

References

Allmann, R.; Hinek, R., 2007.The introduction of structure types into the Inorganic Crystal Structure Database ICSD. Acta Crystallogr. A 63, 412-417.

Atkins, M.; Glasser, F.P.; Kindness, A., 1991. Phase relations and solubility modelling in the CaO-Al2O3-SiO2-MgO-So3-H2O. System for application in blended cements", Proceedings of the Materials Research Society Symposium, Boston, vol. 212, Materials Res. Soc., Pittsburgh, Pennsylvania.

Beltramini, B.; Suarez, M.L.; Guillarducci, A.; Carrasco, M.F.; Grether, R.O., 2010. Aprovechamiento de residuos de la depuración del carbón mineral: Obtención de adiciones puzolánicas para el cemento. Rev. Tecn. y Cien., n. 4, 7-17. (in Spanish).

409 Bonavetti, V.L.; Rahhal, V.F.; Irasser, E.F., 2001. Studies on the
410 carboaluminate formation in limestone filler blended cements. Cem. Concr. Res.
411 31, 853-859.

412 BP Statistical Review of Wold Energy, www.bp.com (2017)

413 Brindley, G.W.,1951. The kaolin minerals X ray identification and structures of
414 clay minerals. Mineralogical Society, London, UK

415 Caglioti, G., Paoletti, A and Ricci, F.P. (1958). Choice of collimators for a crystal
416 spectrometer for neutron diffraction. Nuclear Instrumentation, 3, 223-228.

417 Chakchouk, A.; Samet, B., 2012. Difference in pozzolanic behaviour of Tunisian
418 clays with lime and cement. Adv. Cem. Res. 24,11-22.

419 Dollase, W.A. (1986). Correction of intensities for preferred orientation in
420 powder diffractometry: Application of the March model. Journal of Applied
421 Crystallography 19, 267-272

422 Dontala, S.P.; Reddy, T.B.; Vadde, R., 2015. Environmental aspects and
423 impacts its mitigation measures of corporate coal mining. Procedia Earth
424 Planet. Sci. 11, 2-7.

425 European Committee for Standardization, 2011. EN 197-1. Cement-Part-1:
426 Composition, Specifications and Conformity Criteria for Common Cements.

427 Fan, G.; Zhang, D.; Wang, X., 2014. Reduction and utilization of coal mine
428 waste rock in China; A case study in Tiefa coalfield. Resour. Conserv. Recyc*l*.
429 83, 24-33.

430 Feldman,R.F.; Ramachandran, V.S.; Screda, P.J., 1965. Influence of $CaCO_3$ on
431 the hydration of 3CaO.Al2O3. J. Am. Ceram. Soc. 48, 25-30.

432 Frías, M.; Sánchez de Rojas, M.I., 1997. Microstructural alterations in fly ash
433 mortars study on phenomena affecting particle and pore size. Cem. Concr. Res.
434 27, 619-628.

435 Frías, M., 2006. Study of hydrated phases present in a MK-lime system cured at
436 60ºC and 60 months of reaction. Cem. Concr. Res. 36, 827-831.

437 Frías, M.; Vigil, R.; Sánchez de Rojas, M.I.; Medina, C.; Juan, A., 2012.
438 Scientific aspects of kaolinite based coal mining wastes in pozzolan/$Ca(OH)_2$
439 system. J. Am. Ceram. Soc. 95, 386-391.

440 Frías, M.; Martínez-Ramírez, S.; Blasco, T.; Frías Rodríguez, M., 2013.
441 Evolution of mineralogical phases by ^{27}Si NMR in MK-$Ca(OH)_2$ system cured at
442 60ºC. J. Am. Ceram. Soc. 96, 2306-2310.

443 Frías, M.; Rodriguez, O.; Sánchez de Rojas, M.I., 2015. Paper sludge, an
444 environmental sound alternative source of MK based cementitious Materials. A
445 review. Constr. Build. Mater, 74, 37-48.

446 Frías, M.; Rodriguez, O., Vigil, R.; García, R.; Martínez, S.; Fernández, L.;
447 Vegas, I., 2016. The influence of activated mining wastes on the mineralogy of
448 blended cement pastes. J. Am. Ceram. Soc. 99, 300-307.

449 FullProf. http://www.ill.eu/sites/fullprof/index.html

García, R.; Vigil, R.; Frías, M.; Rodriguez, O.; Martínez, S.; Fernández, L.; de Soto, I.S.; Villar,E., 2015. Mineralogical study of calcined coal waste in a pozoolan/Ca/OH)$_2$ system. Appl. Clay Sci. 108, 45-54.

García, R.; Vigil, R.; Rubio, V.; Frías, M., 2016. The transformation of coal mining waste minerals in the pozzolanic reaction of cements. Minerals, 6, 64.

Goñi, S.; Frías, M.; Vigil, R.; Vegas, I., 2013. Decalcification of activated paper sludge-fly ash- Portland cement blended pastes in pure water. Cem. Concr. Comp. 40, 1-6.

Grazulis, S.; Daskevic, A.; Merkys, A.; Chateigner, D.; Lutterotti, L.; Quirós, M.; Serebryanaya, N. R.; Moeck, P.; Downs, R. T.; Le Bail, A.,2012. Crystallography Open Database (COD): an open-access collection of crystal structures and platform for world-wise collaboration. Nucleic Acids Res. 40, (D1), D420-D427.

Haibin, L.; Zhenling, L., 2010. Recycling utilization patterns of coal mining waste in China. Resour. Conserv. Recycl. 54, 1331-1340.

Juenger, M.C.G., Siddique, R., 2015. Recent advances in understanding the role of supplementary cementitious Materials in concrete. Cem. Concr. Res. 78, 71-80.

Kunther, W.; Dai, Z.; Skibsted, J., 2016. Thermodynamic modelling of hydrated white Portland cement–metakaolin–limestone blends utilizing hydration kinetics from 29Si MAS NMR spectroscopy. Cem. Concr. Res. 86, 29–41.

Match - Phase Identification from Powder Diffraction - Version 3, Crystal Impact - Dr. H. Putz & Dr. K. Brandenburg GbR, Kreuzherrenstr. 102, 53227 Bonn, Germany, http://www.crystalimpact.com/match

Martínez,S.; Frías, M., 2011. Micro-raman study of stable and metastable phases in MK/Ca(OH)2 system cured at 60ºC. Appl. Clay Sci. 51, 283-286.

McCusker, L.B., Von Dreele, R.B., Cox, D.E., Löuer, D. and Scardi, P.,1999. Rietveld Refinement Guidelines. Journal of Applied Crystallography 32, 36-50

Medina, G., Sáez del Bosque, I.F., Frías, M., Sánchez de Rojas, M.I., Medina, C., 2017. Mineralogical study of granite in a pozzolan/Ca(OH)2 system: Influence of the activation process. Appl. Clay Sci.135, 362-371.

Modarres, A.; Ayar, P., 2014. Coal waste application in recycled asphalt mixtures with bitumen emulsion. J.Cleaner Prod. 83, 263-272.

Modarres, A.; Hesami, S.; Soltaninejad, M.; Madani, H., 2017. Application of coal waste in sustainable roller compacted concrete pavement environmental and technical assessment. Int. J. Pavement Eng. Published online, http://dx.doi.org/10.1080/10298436.2016.1205747.

Mohammed, S., Elhem, G., Mekki, B., 2016. Valorization of pozzolanicity of Algerian clay: Optimization of the treatment and mechanical characteristics of the involved cement mortars. Appl. Clay Sci.132-133, 711-721.

Monte, M.C.; Fuente, E.; Blanco, A.; Negro, C., 2009. Waste management from pulp and paper production in the European Union. Waste Manag. 29, 293-308.

Qoku, E., Bier, T.A., Westphal, T., 2017.Phase assemblage in ettringite-forming cement paste: A X-ray diffraction and termal analysis characterization. J. Build. Engin. 12, 37-50.

Rietveld, H.M., 1967. Line profiles of neutron powder-diffraction peaks for structure refinement. Act. Crystal. 22, 151–152.

Rietveld, H.M., 1969. A profile refinement method for nuclear and magnetic structures. J. Appl. Crystal. 2, 65–71.

Rodríguez, O.; Kacimi, L.; López-Delgado, A.; Frías, M.; Guerrero, A., (2013). Characterization of Algarian reservoir sludges for use as active additions in cement: New pozzolans for eco-cement manufacture. Constr. Build. Mater. 40, 275-279.

Sáez del Bosque, I.F.; Martinez-Ramirez, S.; Blanco-Varela,M.T., 2014. FTIR study of the effect of temperature and nanosilica on the nanostructure of C-S-H gel formed by hydrating tricalcium silicate. Constr. Build. Mater. 52, 314-323.

Segui, P.; Aubert, J.E.; Husson, B.; Measson, M., 2012. Characterization of wastepaper sludge ash for its valorisation as a component of hydraulic binders. Appl. Clay Sci. 57, 79-85.

Stark, J., 2011. Recent advances in the field of cement hydration and microstructure analysis. Cem. Concr. Res. 41, 666-678.

Vegas, I.; Gaitero, J.J.; Urreta, J.; García, R.; Frías, M., 2014. Aging and durability of ternary cements containing fly and activated paper sludge. Constr. Build. Mater. 52, 253-260.

Vegas, I.; Cano, M.; Arribas, I.; Frías, M.; Rodriguez, O., 2015. Physical-mechanical behaviour of binary cements blended with thermally activated coal mining waste. Contr. Build. Mater. 99, 169-174.

Vigil, R.; Frías,M.; Sánchez de Rojas, M.I.; Vegas, I.; García, R., 2007. Mineralogical and morphological changes of calcined paper sludge at different temperaturas and retention in furnace. Appl. Clay Sci. 36, 279-286.

Vigil, R.; Frías, M.; García, R.; Martínez, S.; Fernández, L., 2014. Chemical and mineral transformation that occur in wine waste and washery rejects during preutilization calcination. Int. J. Coal Geol. 132, 123-130.

Vigil, R.; García, R.; Martínez, S.; Frías, M., 2017. Effects of calcination temperature and the addition of ZnO on coal waste activation: A mineralogical and morphological evolution. Appl. Clay Sci. 150, 1-9.

Wang, Y., Shao, Y., Darko, M., Whalen, J.K., 2016. Recycling combustion ash for suitable cement production: A critical review with data mining and time series predictive models. Constr. Build. Mater. 123, 673-689.

Wu, Z.; Young, J.F., 1984. Formation of calcium hydroxide from aqueous suspensions of tricalcium silicate. J. Am. Ceram. Soc. 67, 48-51.

Yan, S.; Sagoe-Crentsil, K.; Shapiro, G., 2011. Reuse of the-inking sludge from wastepaper recycling in cement mortar products. J. Environ. Mang. 92, 2085-2090.

Yu, P.; Kirkpatrick, R.J.; Poe, B.; McMillan, P.F.; Cong, X., 1999. Structure of Calcium Silicate Hydrate (C-S-H): nearmid and, far infra-red spectroscopy. J. Am. Ceram. Soc. 82, 742-748.

Zajac, M.; Rossberg, A.; Saout, G.L.; Lothenbach, B., 2014. Influence of limestone and anhydrite on the hydration of Portland cements. Cem. Concr. Comp. 46, 99-108.

Figure Captions:

Fig. 1. XRD patterns for 180 d pastes

Fig. 2. 180 d paste morphologies: left: OPC; right, 20%ACW

Fig. 3. 180 d paste morphologies: left, 30%ACW; right, 50%ACW

Fig. 4. 180 d paste morphologies: left, 20%ACW; right, 50%ACW

Fig. 5. EDX analysis of mineralogical phases

Fig. 6. FTIR spectra for 180d cement pastes

Fig. 7. Variation in the position of the Q^2 band in C-S-H gel with increasing waste content

Fig. 8. ^{29}Si spectra for 180 d cement pastes.

Fig. 9. ^{27}Al NMR spectra for 180 d cement pastes

Fig. 10. Evolution of DTG diffractograms for OPC and 50% OPC pastes with hydration time

Fig. 11. Bound water and portlandite contents in cement pastes versus OPC replacement ratio and hydration time

Highlights

The present paper shows new knowledges in low clinker cement manufacture

This paper studies the influence of high contents of clay waste in the mineralogy of cement pastes cured up to 180d.

ACW favoured the formation of C_4AH_{13} over C_4AcH_{12}

ACW favoured the compact C-S-H gel plates, and phyllosilicate-like laminar spongy microplates.

Table

Click here to download Table: revised tables.docx

Table I. Chemical compositions (%) of OPC and ACW

Materials	SiO_2	Al_2O_3	Fe_2O_3	CaO	MgO	K_2O	Na_2O	SO_3	TiO_2	P_2O_5	LOI
OPC	20.80	5.70	2.89	58.99	1.89	1.36	0.93	4.11	0.15	0.26	2.79
ACW	52.63	25.29	4.64	4.20	0.77	3.09	0.17	0.27	1.17	0.14	3.09

Table II. Rietveld analysis of XRD-identified phases

Phases (%)		CF	Bs	C3	Al	Br	Ca	Q	M	K	Et	P	Am	Cc	C4A	X^2
	OPC	8	7	15	35	25	1	0	0	0	0	0	9	0	0	15.4
	CW	0	0	0	0	0	15	29	25	14	0	0	17	0	0	5.7
	ACW	0	0	0	0	0	10	35	20	0	0	0	35	0	0	6.9
1d	OPC	2	1	7	12	20	4	0	0	0	12	32	10	0	0	14.7
	20%	0	0	0	3	11	18	7	4	0	9	37	11	0	0	9.7
	30%	0	0	0	3	7	7	10	4	0	7	15	47	0	0	6.8
	50%	0	0	0	3	5	5	22	10	0	5	10	40	0	0	6.7
7d	OPC	1	0	4	4	18	13	0	0	0	15	29	13	3	0	8.6
	20%	0	0	0	0	10	10	9	3	0	12	27	10	4	15	9.7
	30%	0	0	0	0	8	8	13	5	0	9	25	15	7	10	8.7
	50%	0	0	0	0	6	4	19	9	0	6	16	25	6	9	7.0
28d	OPC	0	0	0	1	17	11	0	0	0	15	25	10	14	7	7.6
	20%	0	0	0	0	7	9	9	3	0	9	23	9	11	20	4.5
	30%	0	0	0	0	6	9	10	5	0	7	14	19	10	20	5.4
	50%	0	0	0	0	4	5	19	8	0	5	9	27	5	18	9.4
90d	OPC	0	0	0	0	2	9	0	0	0	11	24	30	17	7	10.2
	20%	0	0	0	0	0	10	15	3	0	9	22	11	12	18	12.3
	30%	0	0	0	0	0	8	19	6	0	7	19	18	9	14	6.0
	50%	0	0	0	0	0	4	23	8	0	5	16	25	7	12	8.3
180d	OPC	0	0	0	0	2	7	0	0	0	10	22	40	15	4	8.6
	20%	0	0	0	0	0	14	12	3	0	7	20	21	10	13	9.7
	30%	0	0	0	0	0	13	17	8	0	5	15	23	9	10	8.7
	50%	0	0	0	0	0	12	22	9	0	4	5	31	8	9	7.0

CF=C4AF; Bs = bassanite; C3 = C3A; Al =C3S; Br = C2S; Ca = calcite; Q = Quartz; M=mica;. K= kaolinite; Et = ettringite; P = portlandite; Cc=C4AC H12; C4A=C4H13; Am. Mat = Amorfous.

Table III: Datasets for phase identification and Rietveld quantification

Phases	COD*	ICSD**
Alite	9016125	
Calcite	9007689	
Quartz	9012600	
C_4AcH_{12}	2007668	
Ettringite	9011103	
Mica (Fengite)	9005496	
Portlandite	1008781	
Rutile	9007433	
C_4AH_{13}	-	00-042-0558
Bredigite	9000483	
C4AF	1008124	
Bassanite	9005521	
C3A	1000039	

*COD: Crystallography Open Database, **ICSD: Inorganic Crystal Structure Database

Table IV: Chemical analysis by EDX of blended cements at 180days

oxides	20 % C-S-H gel	30% C-S-H gel	30% plate	50% C-S-H gel	50% plate
MgO	0.6±0.46	1.1±0.63	0.6±0.15	1.4±0.48	1.4±0.42
Al_2O_3	6.7±0.94	6.2±0.89	20.2±0.96	9.2±0.62	21.1±0.77
SiO_2	31.5±2.59	36.3±2.85	38.8±1.46	37.1±2.59	45.3±2.38
SO_3	2.8±0.43	1.9±0.53	2.4±0.62	-	3.6±0.71
CaO	56.7±1.85	53.2±2.21	36.7±2.25	50.6±1.97	27.4±1.62
Fe_2O_3	1.8±0.32	1.2±0.19	1.4±0.24	1.6±0.74	1.2±0.18

Figure 1

Click here to download high resolution image

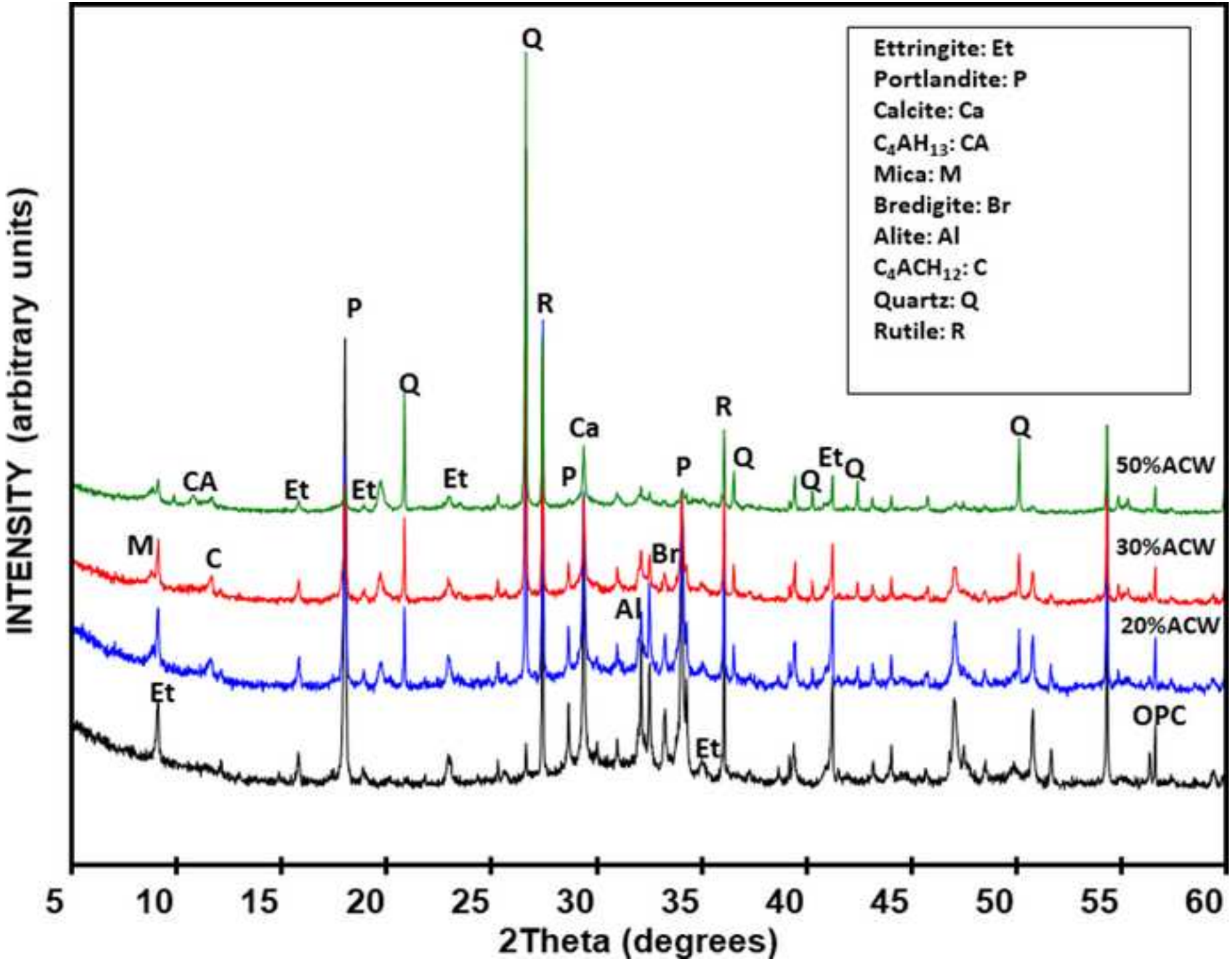

Figure 2

Click here to download high resolution image

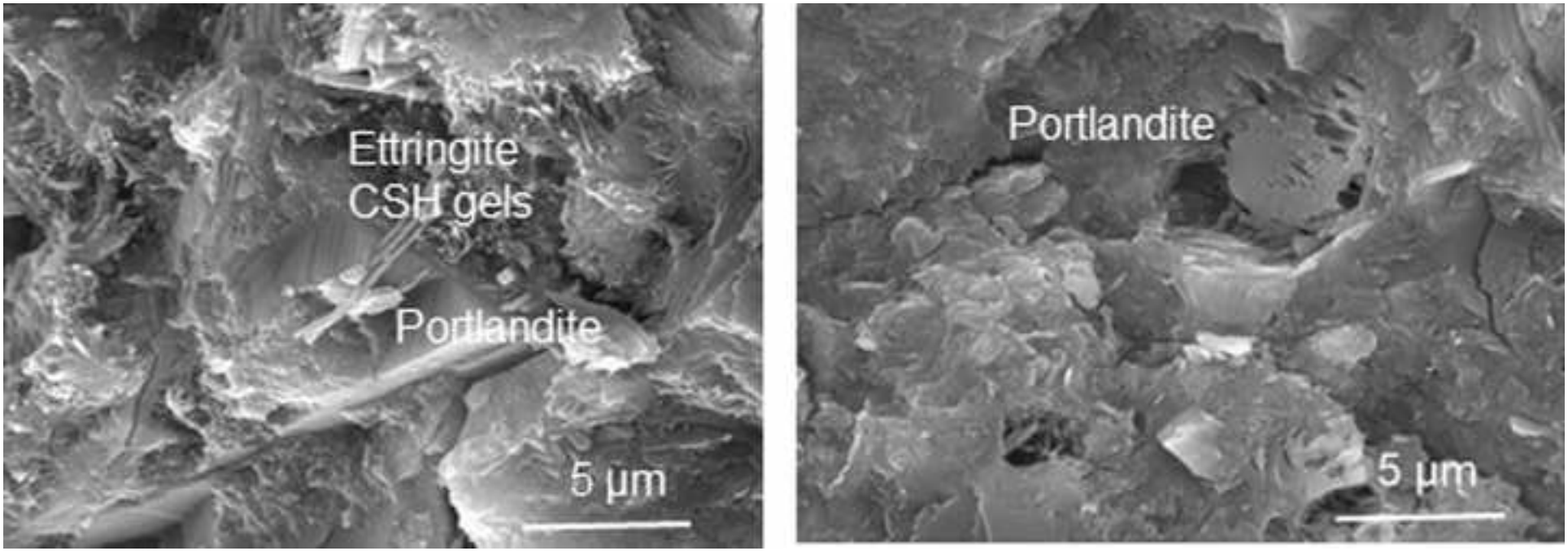

Figure 3

Click here to download high resolution image

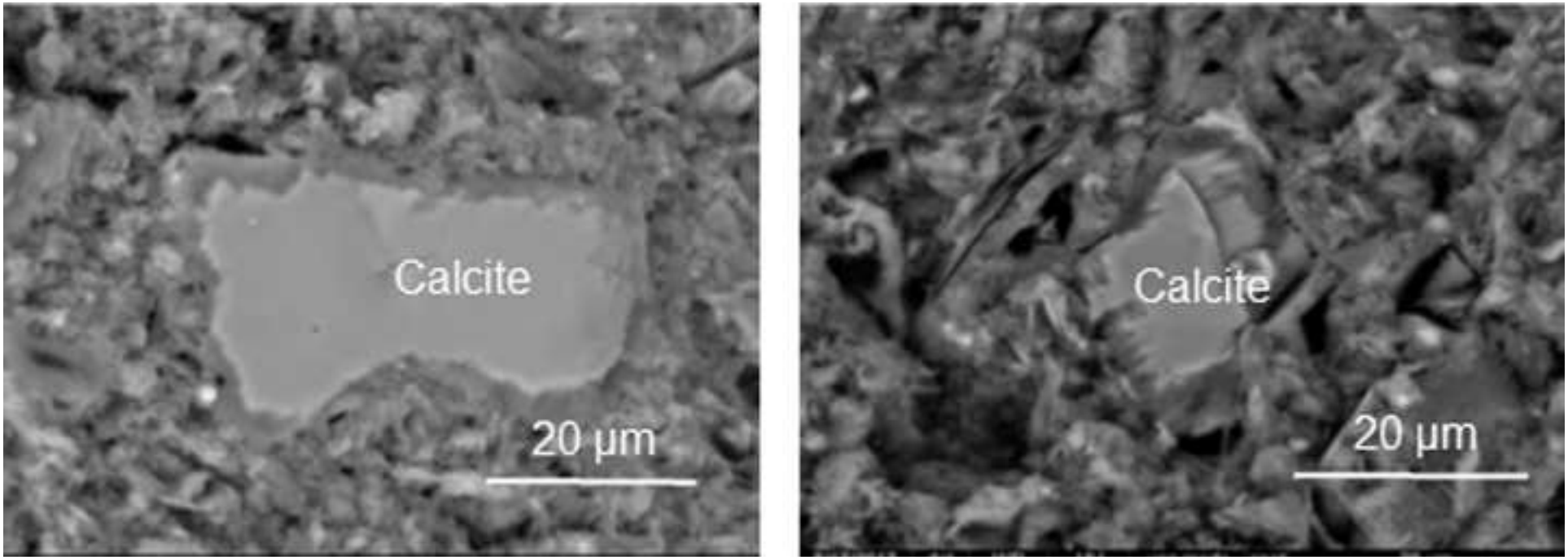

Figure 4

Click here to download high resolution image

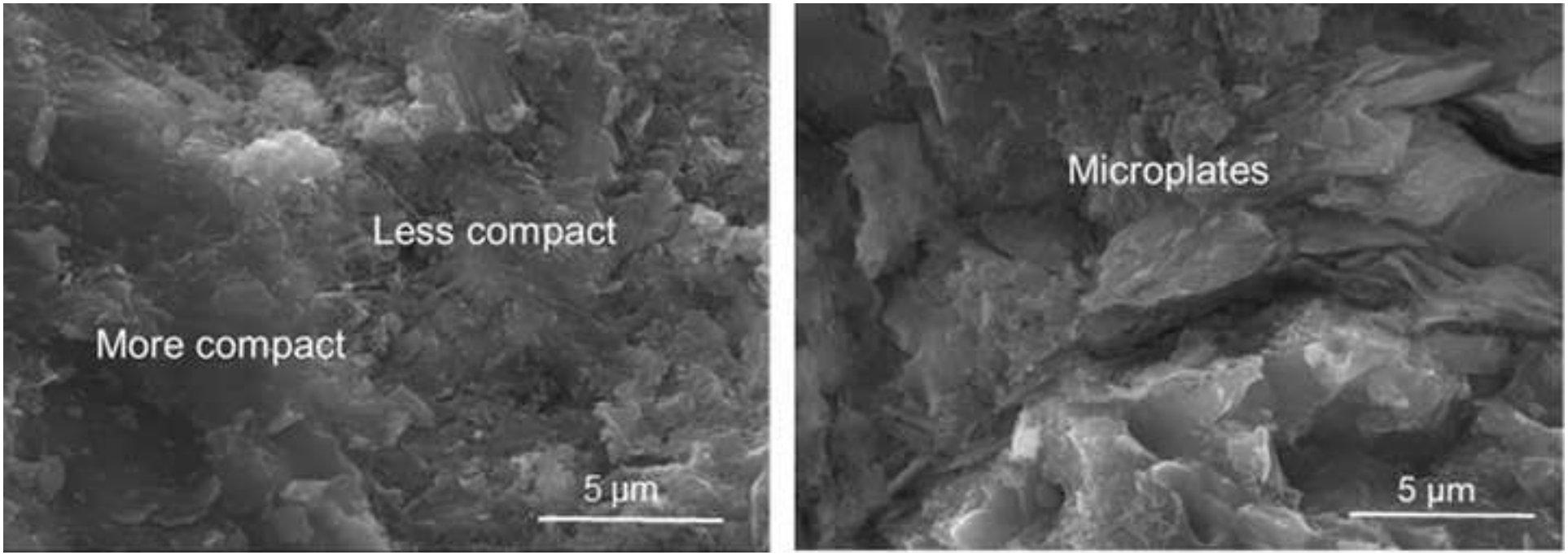

Figure 5

Click here to download high resolution image

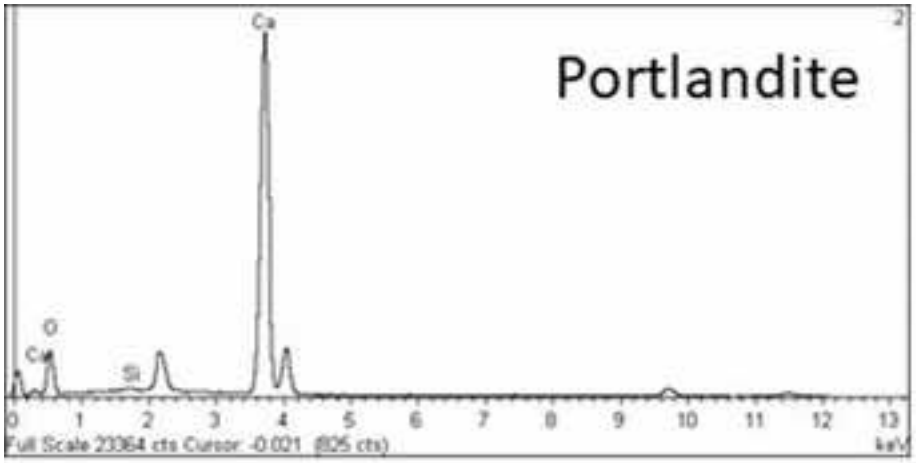

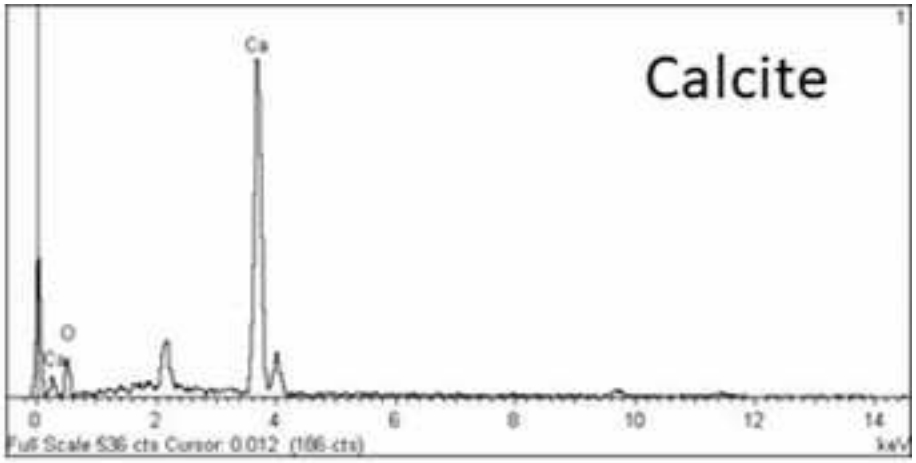

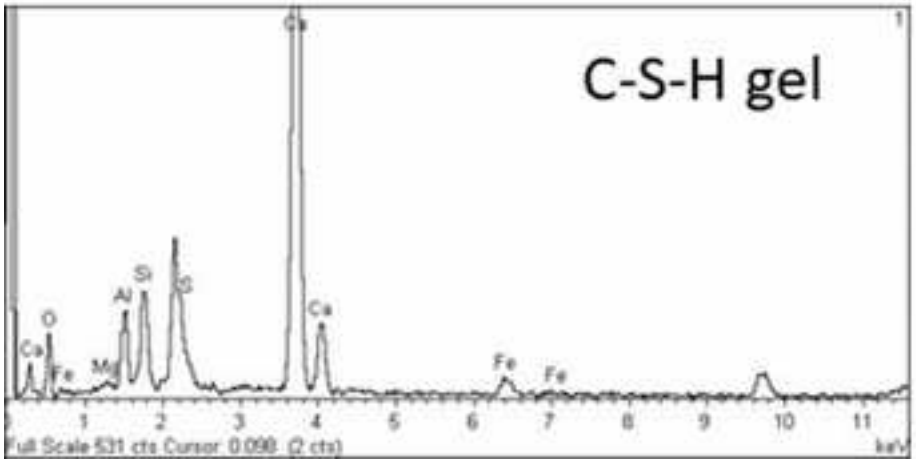

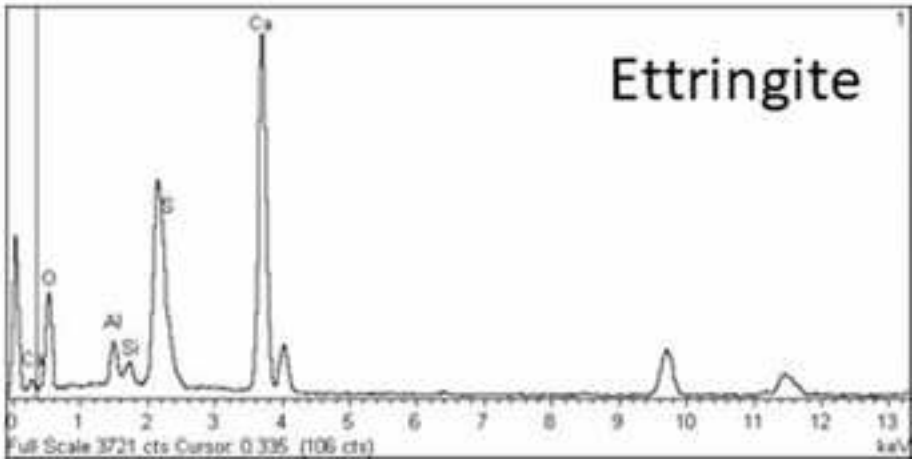

Figure 6

Click here to download high resolution image

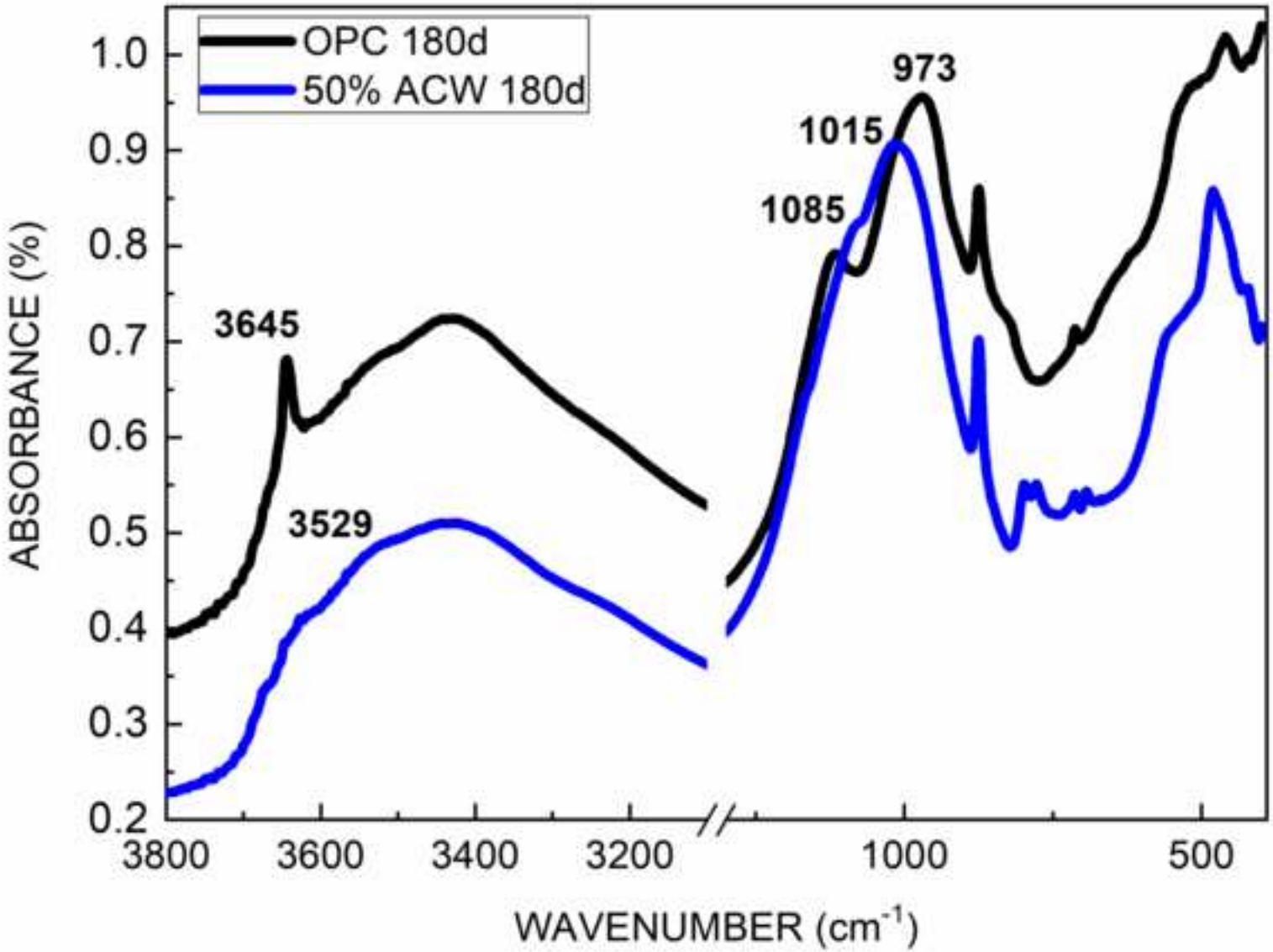

Figure 7
Click here to download high resolution image

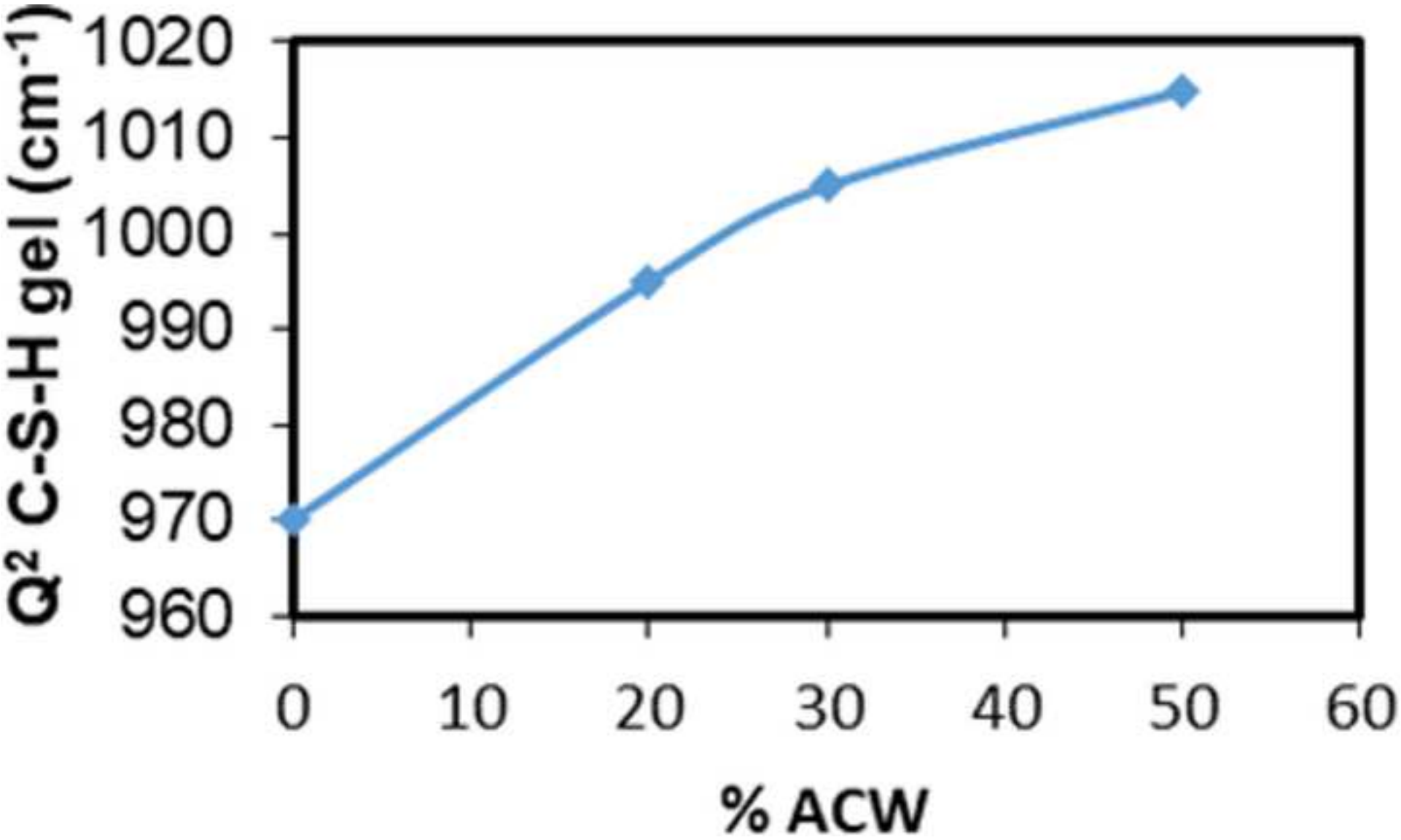

Figure 8

Click here to download high resolution image

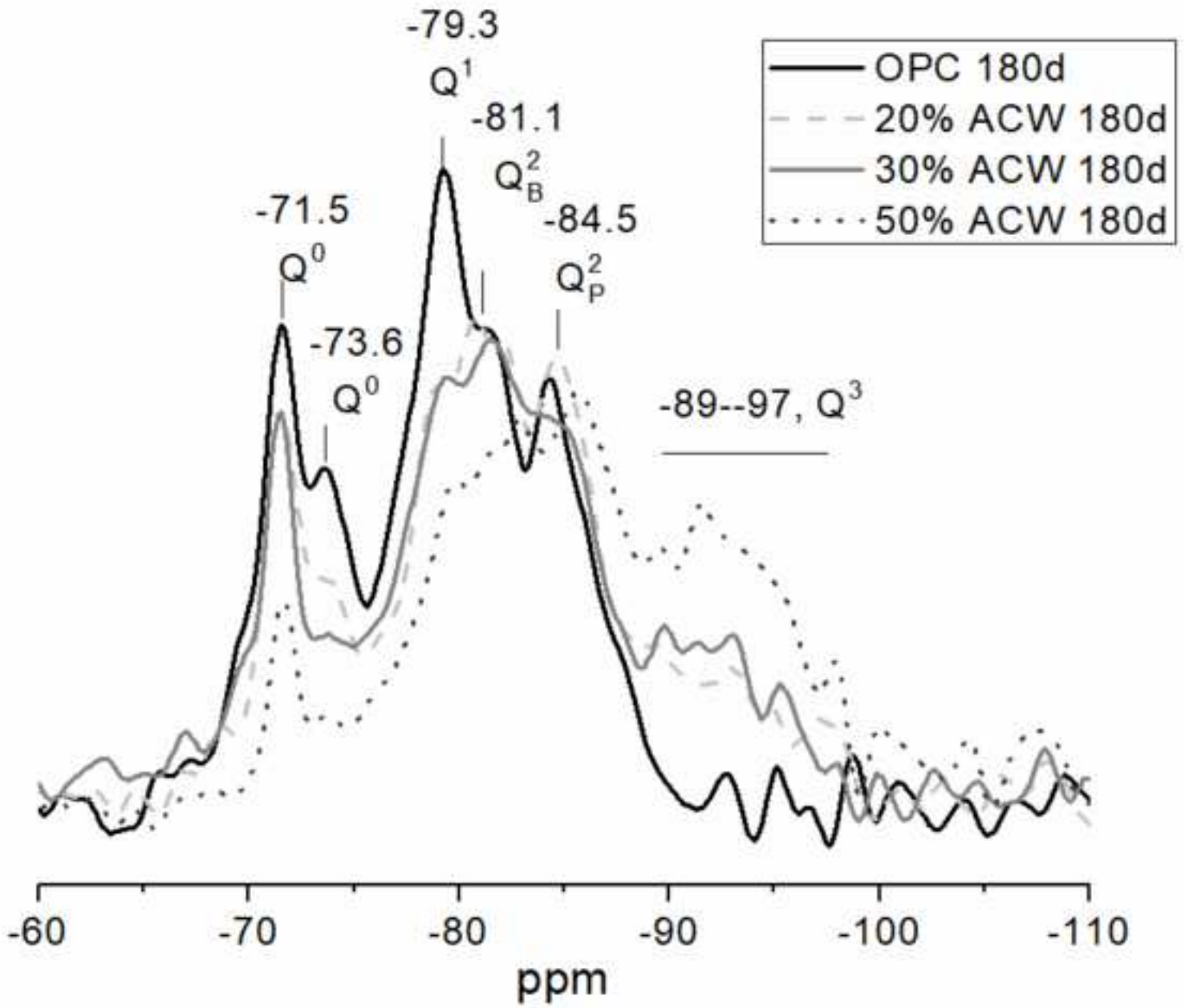

Figure 9

Click here to download high resolution image

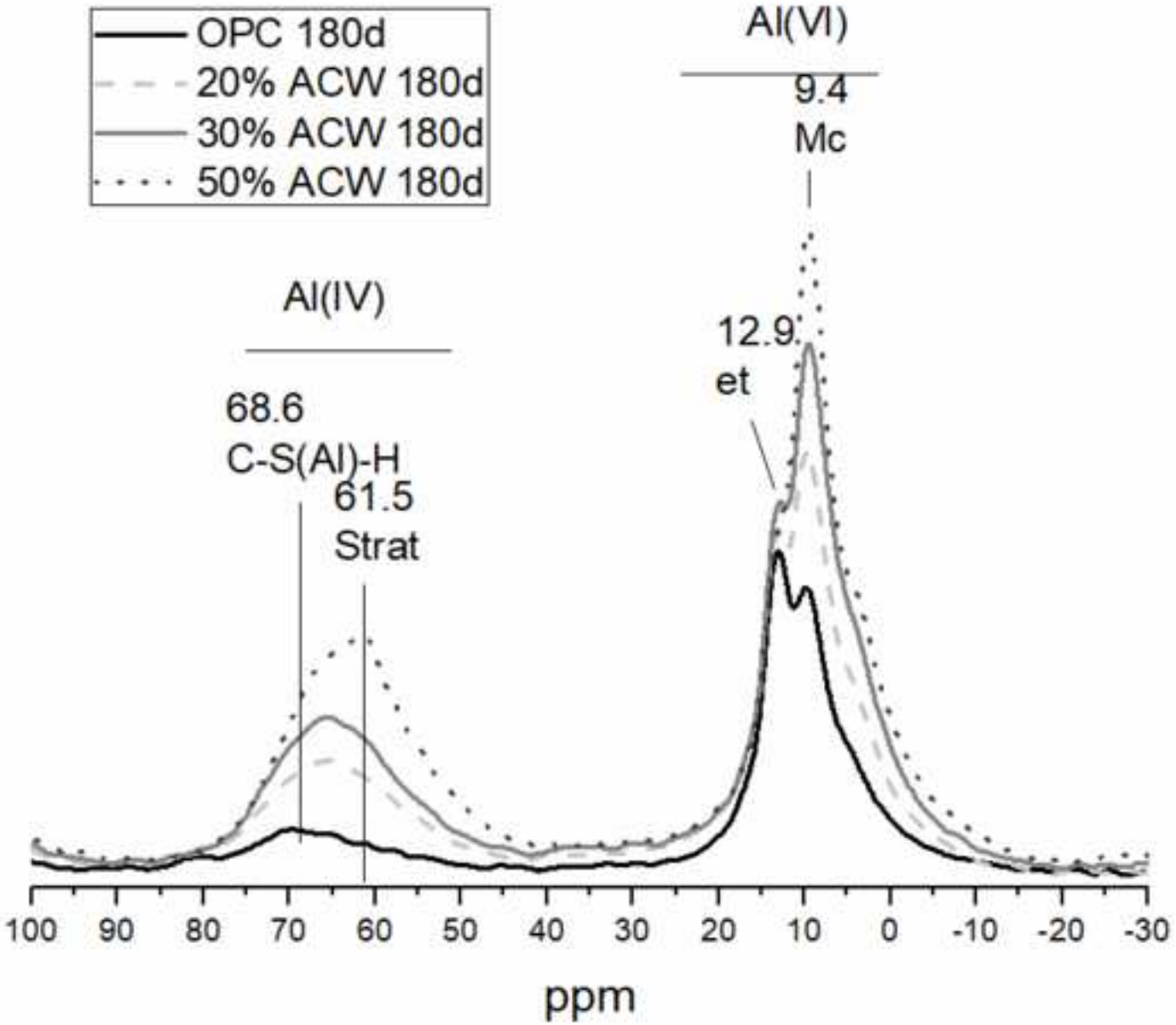

Figure 10

Click here to download high resolution image

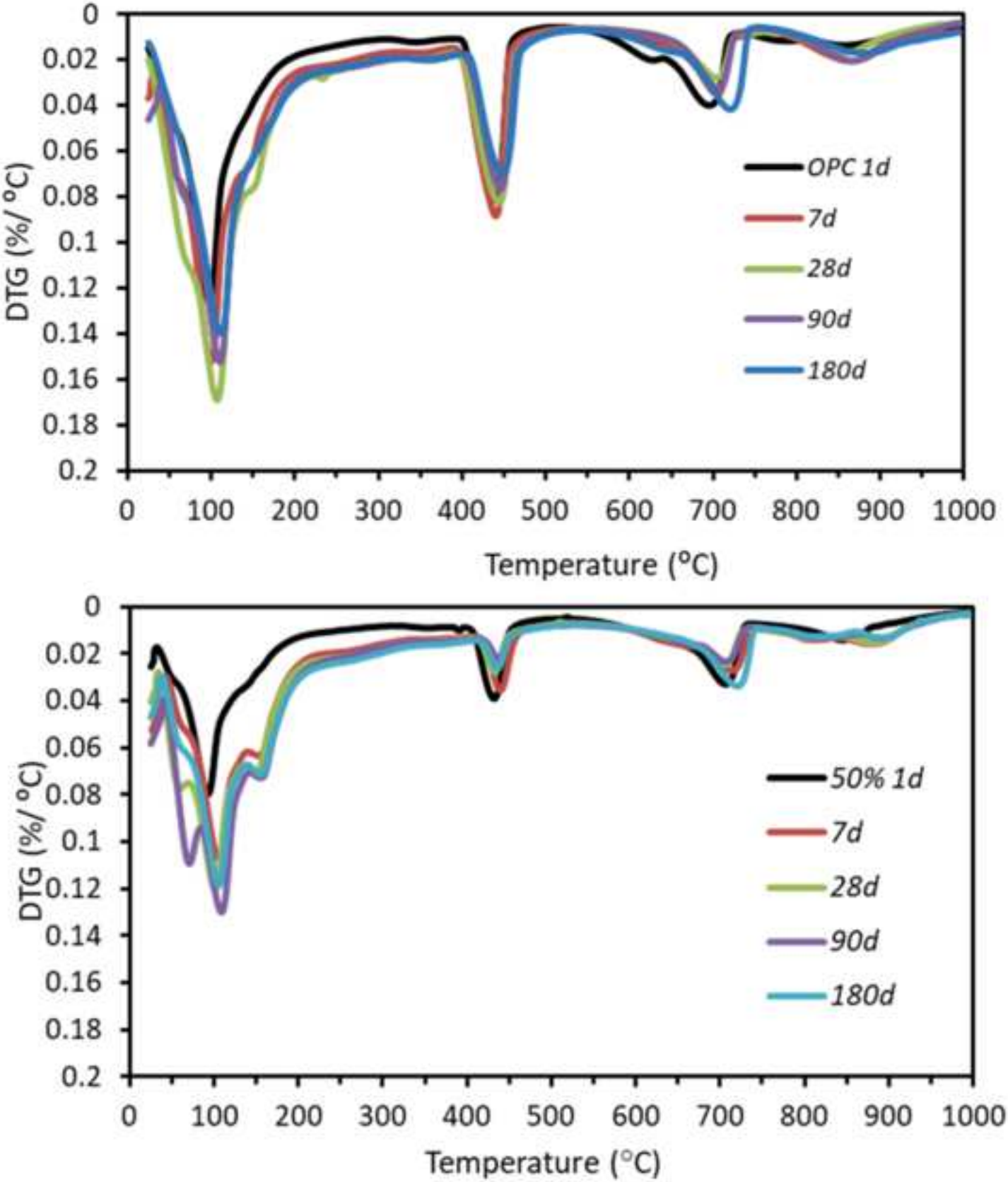

Figure 11

Click here to download high resolution image

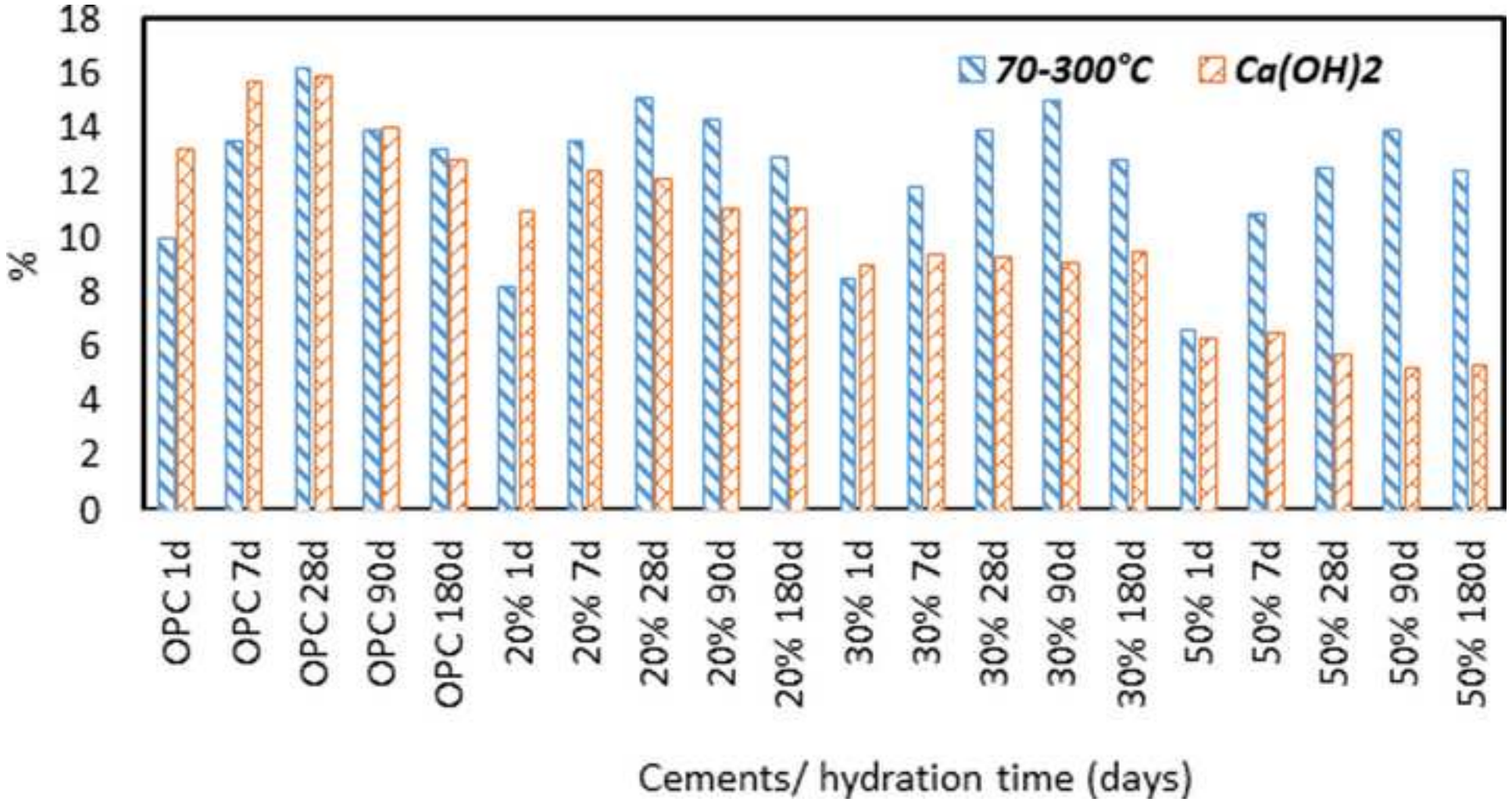

***Abstract**

Click here to download Abstract: Revised Abstract.docx

The use of industrial waste as a cement addition often changes the composition and development of the hydrated phases and with them matrix performance and durability, in particular at later ages. The effect of the presence in blended cement of 20% to 50% Kaolinite based activated carbon waste (ACW) on paste hydration has been characterized by means of XRD, SEM/EDX, TG/DTG, NMR and FTIR to identify and monitor the mineralogical phases forming in materials at ages of up to 180 d. The results showed that the main reaction products forming in the first 7 d included C-S-H gels, C_4ACH_{12} and C_4AH_{13} (hydroxy-AFm). Whilst monocarboaluminate (Mc) content declined with rising percentages of ACW, the amount of hexagonal phase hydroxy-AFm rose generally speaking. Then microstructure of the C-S-H gels developing in the OPC and the 50% additioned paste differed. Compact C-S-H gel plates, and phyllosilicate-like laminar spongy microplates with high polymerised C-S-H gel formed in the blended cement paste.